

A study of the core of the Shapley Concentration: V. The A3528 complex: a young merger event? [★]

Sandro Bardelli¹, Elena Zucca¹ & Alessandro Baldi²

¹ *Osservatorio Astronomico di Bologna, via Ranzani 1, I-40127 Bologna, Italy*

² *Dipartimento di Astronomia, Università degli Studi di Bologna, via Ranzani 1, I-40127 Bologna, Italy*

E-mail: bardelli@bo.astro.it, zucca@bo.astro.it

Received 00 - 00 - 0000; accepted 00 - 00 - 0000

ABSTRACT

We present the results of a redshift survey of galaxies in the A3528 complex, a chain of interacting clusters in the core of the Shapley Concentration. This complex is characterized in the X-ray band by two pairs of roughly similar interacting clumps: one pair has been resolved as two optical Abell clusters (A3530 and A3532), while the two components of the other pair are both associated to A3528. The optical data show that the distance between the centers of A3530 and A3532 is smaller than their Abell radii, an indication of the existence at least of tidal interactions, and that the contours of galaxies in A3528 appear to be elongated in the North–South direction, pointing towards the A3530–A3532 pair.

From our survey we obtained ~ 600 new radial velocity determinations: using this sample, we studied the dynamics of the four Abell clusters in this region (A3528, A3530, A3532 and A3535) and derived their mean velocities and velocity dispersions. Moreover we performed a substructure analysis, both bi-dimensional and three-dimensional, of the whole complex.

All the characteristics of this structure seem to point toward a merging scenario in an early stage, whose effects on the galaxy population and on the cluster dynamics are not yet evident, contrary to what happens in the nearby A3558 complex, where the merging events are in a rather advanced stage and were already able to induce modifications in the galaxy population.

Key words: galaxies: distances and redshifts – galaxies: clusters: general – galaxies: clusters: substructures – galaxies: clusters: individuals: A3528 - A3530 - A3532 - A3535

1 INTRODUCTION

Clusters of galaxies are thought to form by accretion of subunits in a hierarchical bottom-up scenario (see f.i. Colberg et al. 1998): the fact that substructures are observed in a high fraction of clusters (see f.i. Bird 1994) indicates that this accretion phenomenon is still active.

Cluster mergings are among the most energetic phenomena in the Universe, leading to a release of $\sim 10^{50-60}$ ergs in a time scale of the order of Gyrs. The astrophysical consequences of this energy output are expected to be both thermal (shocks, changes in the temperature and gas distribution profiles of the Intra Cluster Medium) and non-thermal (appearance of radio sources like Halos or Relics, hard X-ray tails). Such effects are visible at different wavelengths, but

while the merging event is rather well studied in the X-ray band, the studies of the velocity distribution and morphological modification of the galaxy population suffered until recently by the limited number of available spectra per cluster. A significant improvement in this field will be achieved by the new generation of multi-fiber spectrographs, which allow to obtain hundreds of spectra simultaneously. However, even with the “old” multi-fiber spectrographs like OPTOPUS and MEFOS it has been possible to map major merger events like the A3558 complex in the core of the Shapley Concentration (Bardelli et al. 1994, 1998a, 1998b, 2000), as part of a large, multiwavelength project.

The Shapley Concentration is a unique laboratory where to study the cluster merging because, given the high local overdensity (of the order of ~ 10 on scales of 10 h^{-1} Mpc, Bardelli et al. 2000), the induced peculiar velocities increase the “cross section” for cluster-cluster collisions. In particular, two clusters complexes are found at the cen-

[★] based on observations collected at the European Southern Observatory, La Silla, Chile.

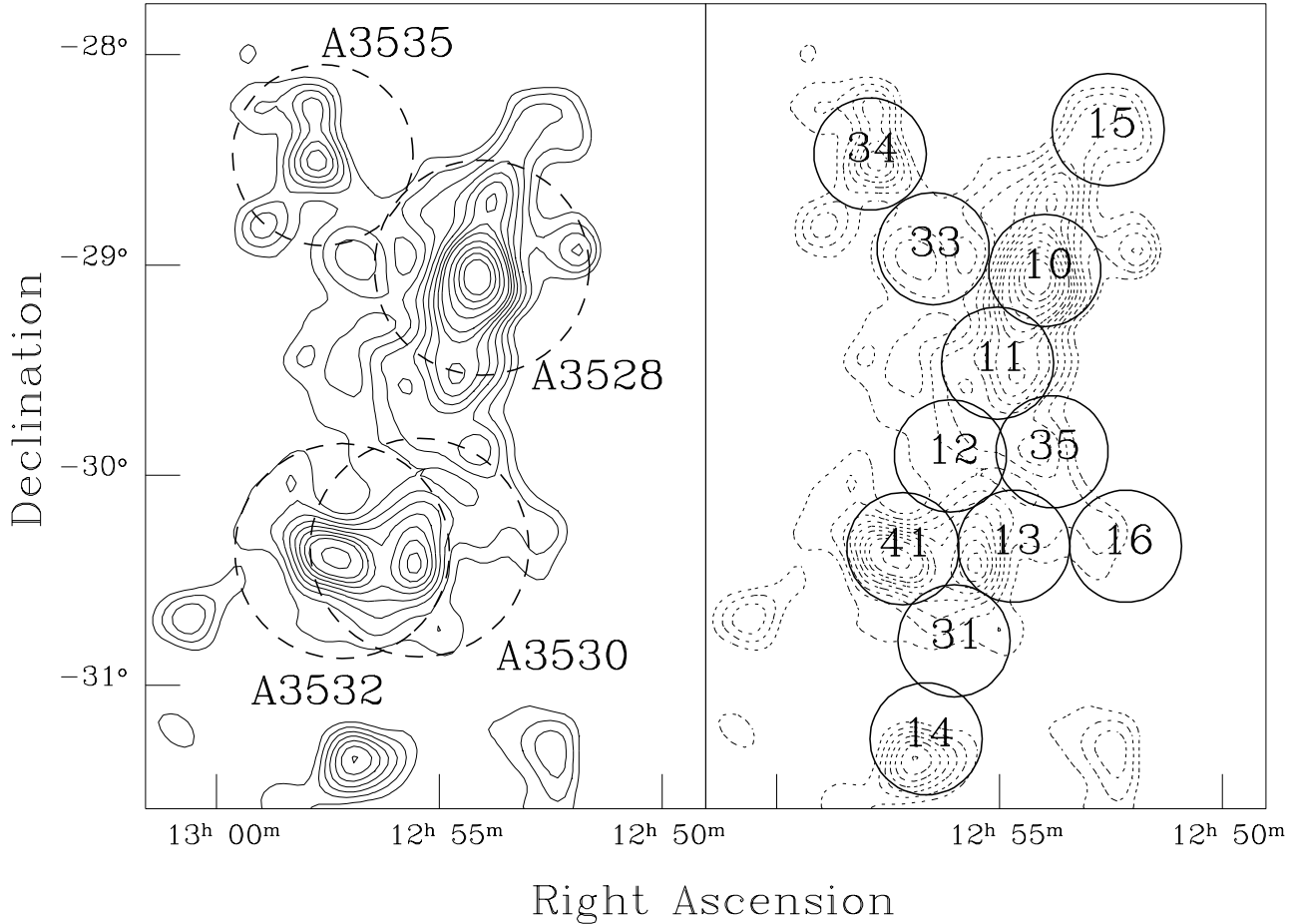


Figure 1. Left: Isodensity contours of galaxies in an area of $\sim 2.7 \times 3.8$ around the A3528 cluster complex. The figure refers to galaxies in the magnitude range 17 – 19.5 and the data have been binned in 2×2 arcmin² bins and smoothed with a Gaussian with a FWHM of 6 arcmin. For the four ACO clusters in the region circles of one Abell radius have been drawn (dashed curves). Right: The same as left panel with superimposed the observed OPTOPUS fields.

ter of the supercluster (Zucca et al. 1994), dominated by A3558 and A3528 respectively: these structures, whose spatial scales are of the order of $\sim 5 \text{ h}^{-1} \text{ Mpc}$ (Bardelli et al. 2000), are formed by strongly interacting clusters. The complex dominated by A3558 has been extensively studied in optical (Bardelli et al. 1994, 1998a, 1998b), radio (Venturi et al. 1997, 1998a, 2000) and X-ray (Bardelli et al. 1996, Ettori et al. 2000) bands, revealing its complex dynamical activity. We suggested that this structure could be the remnant of a cluster-cluster collision seen just after the first core-core encounter.

We are carrying on an analogous multiwavelength study on the complex formed by the ACO (Abell, Corwin & Olowin, 1989) clusters A3528, A3530, A3532 and A3535, which appears very similar to the A3558 complex. These two complexes are separated by $\sim 19 \text{ h}^{-1} \text{ Mpc}$ and are connected by a bridge of galaxies (Bardelli et al. 2000). In this paper we present the results of a dynamical and sub-structure analysis of the clusters in this complex, based on ~ 600 new velocity determinations.

The plan of the paper is the following: in Sect. 2 we present the characteristics of the A3528 complex and in Sect. 3 we describe our galaxy sample. In Sect. 4 we derive the dynamical parameters of the clusters and in Sect. 5 we analyze their substructures. Finally the results are discussed in Sect. 6.

2 THE A3528 CLUSTER COMPLEX

Fig. 1 shows the galaxy isodensity contours in the sky region covering the A3528 complex. This figure shows two interesting features: a) the distance between the centers of A3530 and A3532 is smaller than their Abell radii, an indication of the existence at least of tidal interactions; b) the contours of galaxies in A3528 appear to be elongated in the North–South direction, pointing towards the A3530–A3532 pair. The complex extends for ~ 2.8 degrees in the North–South and ~ 1.7 degrees in the East–West directions, corresponding to linear sizes of $\sim 8 \text{ h}^{-1} \text{ Mpc}$ and $\sim 5 \text{ h}^{-1} \text{ Mpc}$,

respectively, at the mean redshift of the structure (see below).

The cluster A3528 ($\alpha_{2000} = 12^h 54^m 34^s$, $\delta_{2000} = -29^\circ 08' 30''$) is of richness class 1: all the other clusters of the complex are of richness class 0. Quintana et al. (1995) found a mean velocity of $\langle v \rangle = 15631 \pm 148$ km/s and a velocity dispersion of $\sigma = 864_{-85}^{+119}$ km/s determined with 39 galaxies. The ENACS project estimated for this cluster $\langle v \rangle = 15780$ km/s and $\sigma = 969$ km/s, using 28 galaxies (Mazure et al. 1996).

From a ROSAT PSPC observation, Schindler (1996) found that this cluster is actually double, formed by two subcomponents (dubbed A3528N and A3528S) showing an indication of interaction. In fact, the gas seems to be hotter in the region between the two subclusters. Henriksen & Jones (1996) estimated an hot gas temperature of 2.7 ± 0.8 and 2.9 ± 0.9 keV for A3528N and A3528S, respectively. The core radii are 88 ± 10 and 58 ± 5 h⁻¹ kpc, while the total masses are 3.1 and 3.9×10^{13} h⁻¹ M_⊙. Radio observations of this cluster (Schindler 1996; Reid, Hunstead & Pierre 1998; Venturi et al. 1998b) show that in this cluster and in its proximities a large number of extended radio galaxies is located, sign of dynamical activity.

The cluster A3530 ($\alpha_{2000} = 12^h 55^m 31^s$, $\delta_{2000} = -30^\circ 19' 53''$) has an estimated mean velocity of $\langle v \rangle = 15850 \pm 165$ km/s and a velocity dispersion of $\sigma = 643_{-88}^{+146}$ km/s, based on 18 galaxies (Quintana et al. 1995). White, Jones & Forman (1997) reported for this cluster a temperature for the hot gas of 3.2 keV and Ettori, Fabian & White (1997) estimated a total mass of 1.13×10^{14} h⁻¹ M_⊙.

The estimated mean velocity and dispersion of the cluster A3532 ($\alpha_{2000} = 12^h 57^m 22^s$, $\delta_{2000} = -30^\circ 22' 03''$) are $\langle v \rangle = 16085 \pm 102$ km/s and $\sigma = 594_{-58}^{+82}$ km/s, respectively, based on 39 galaxies (Quintana et al. 1995). White et al. (1997) reported a temperature of 4.4 ± 1.5 keV and Ettori et al. (1997) a total mass of 1.7×10^{14} h⁻¹ M_⊙.

The cluster A3535 ($\alpha_{2000} = 12^h 57^m 48^s$, $\delta_{2000} = -28^\circ 29' 18''$), is the least studied of the complex. The only data available in the literature concern its redshift: on the basis of 4 radial velocities Vettolani et al. (1990) estimated a mean velocity of 19770 km/s.

3 THE GALAXY SAMPLE

Fig. 1 shows the isodensity contours for the objects in the magnitude bin $17 \leq b_J \leq 19.5$ from the COSMOS/UKSTJ galaxy catalogue (Yentis et al. 1992), in a region of $\sim 2^\circ.7 \times 3^\circ.8$, corresponding to $12^h 51^m < \alpha_{2000} < 13^h 15^m$ and $-31^\circ 36' < \delta_{2000} < -28^\circ 00'$. This region is part of the plate 443, nearby the border with the plate 442, which is located on the West. The data have been binned in cells of 2×2 arcmin² and then smoothed with a Gaussian with 6 arcmin of FWHM. In the left panel, circles of one Abell radius have been drawn on the four Abell clusters. In the right panel, the positions of the observed OPTOPUS fields are shown. In Table 1 the coordinates and the observation dates of the fields are reported.

Table 1. Centers of the observed OPTOPUS fields

Field	α (2000)	δ (2000)	Obs. Date
10	12 54 18	-29 01 00	8/9-Mar-1991
11	12 55 15	-29 28 42	24/27-Feb-1993
12	12 56 16	-29 55 12	24-Feb-1993
13	12 54 20	-30 21 00	22/27-Feb-1993
14	12 56 45	-31 16 00	26-Feb-1993
15	12 52 54	-28 22 88	27-Feb-1993
16	12 52 54	-30 21 00	26-Feb-1993
31	12 56 09	-30 48 00	27-Feb-1993
33	12 56 42	-28 56 00	25-Feb-1993
34	12 58 05	-28 29 00	23/26-Feb-1993
35	12 54 02	-29 54 00	25-Feb-1993
41	12 57 00	-30 21 42	26-Feb-1993

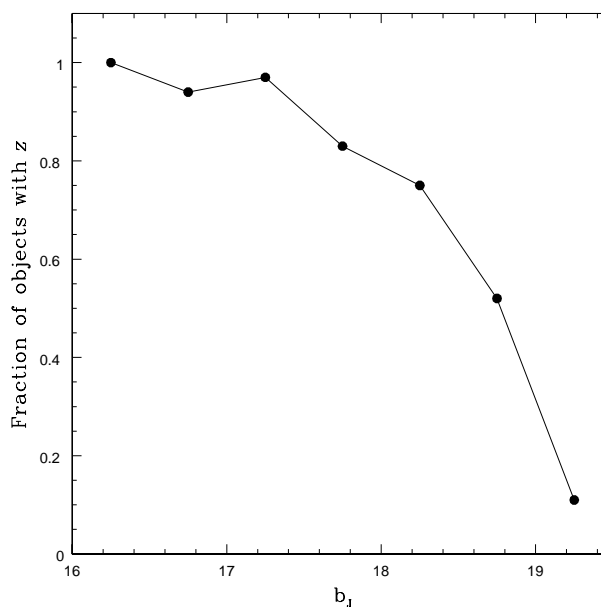


Figure 2. Redshift completeness of the spectroscopic sample as a function of magnitude. Note that the first bin refers to all galaxies with $b_J < 16.5$.

3.1 Observations and data reduction

The spectroscopic observations were performed at the 3.6m ESO telescope at La Silla, equipped with the OPTOPUS multifiber spectrograph (Lund 1986), on the nights of 8 and 9 March 1991 (for the field # 10) and from 23 to 27 February 1993. Fields # 10, # 11, # 13 and # 34 have been observed twice given the high density of galaxies and/or lack of velocity determination in the literature.

The OPTOPUS multifiber spectrograph uses bundles of 50 optical fibers, which can be set within the field of the Cassegrain focal plane of the telescope; this field has a diameter of 32 arcmin, and each fiber has a projected size on the sky of ~ 2.5 arcsec. We used the ESO grating # 15 (300 lines/mm and blaze angle of $4^\circ 18'$) allowing a dispersion of 174 Å/mm (corresponding to a resolution of ~ 12 Å) in the wavelength range from 3700 to 6024 Å. The detectors were

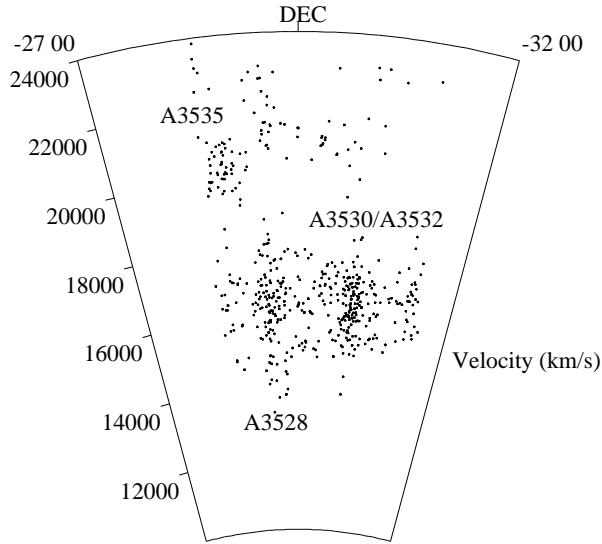


Figure 3. Wedge diagram for galaxies in the velocity range 11000 – 24000 km/s. The diagram is compressed in right ascension and displayed in declination, in order to better visualize the structure.

Tektronic 512×512 CB CCDs (ESO #16 for 1991 run; ESO #32 for 1993 run) with a pixel size of $27 \mu\text{m}$, corresponding to 4.5 \AA , i.e. a velocity bin of $\sim 270 \text{ km/s}$ at 5000 \AA . Detector #32 has a particularly good responsive quantum function in the blue ($\sim 70\%$ at 4000 \AA), where there are the calcium and [OII] lines.

Following Wyse & Gilmore (1992), we dedicated 5 fibers to sky measurements, remaining with 45 fibers available for the objects. The observing time for each field was one hour, split into two half-hour exposures in order to minimize the effects due to the “cosmic” hits. The observing sequence was: a 30 seconds exposure of a quartz–halogen white lamp, a 180 seconds exposure of the Phillips Helium and Neon arcs, then the first and the second field exposures, and again the arcs and the white lamp.

The reduction steps are described in Bardelli et al. (1994). However, it could be important to stress that we normalized the fiber transmission dividing each spectrum by the continuum-subtracted flux of the sky emission line [OI] λ 5577. This procedure assumes that the sky emission does not change significantly on angular scales of the order of $\sim 30 \text{ arcmin}$ (Wyse & Gilmore 1992).

We obtained estimates of the radial velocity of galaxies using the cross-correlation method as implemented in the IRAF[†] task RVSAO (XCSAO, Kurtz et al. 1992). The galaxy spectra were cross-correlated with those of 8 stellar templates observed with the same instrumental set up. The adopted velocity for each galaxy is the value given by the template which gives the minimum cross-correlation error. For spectra with strong emission lines we measured an

[†] IRAF is distributed by KPNO, NOAO, operated by the AURA, Inc., for the National Science Foundation.

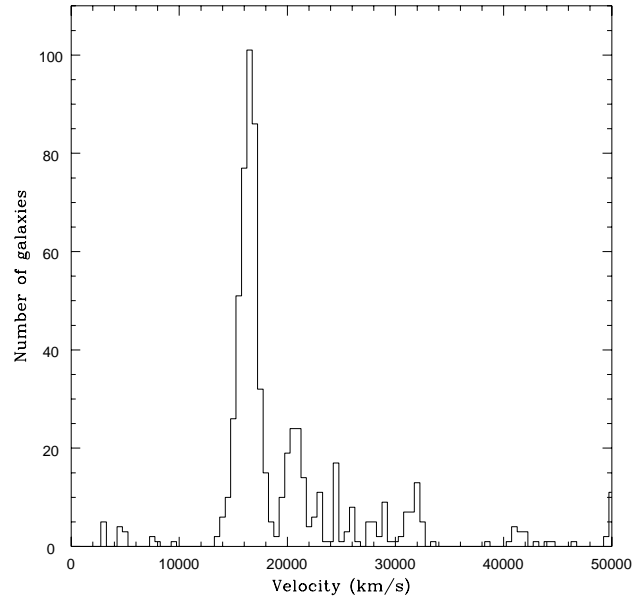


Figure 4. Velocity histogram of the galaxies in the range 0 – 50000 km/s: the main peak at $\sim 16000 \text{ km/s}$ corresponds to A3528, A3530 and A3532, while the peak at $\sim 20000 \text{ km/s}$ corresponds to A3535.

“emission velocity” using the EMSAO program in the same IRAF task RVSAO.

3.2 The new redshift data

From the total number of spectra (692), it was possible to obtain 662 velocity estimates: 81 objects turned out to be stars ($\sim 12\%$ of the reliable spectra), leaving us with 581 new galaxy redshifts.

In Table 2 we list the objects with velocity determination. Columns (2), (3) and (4) give the right ascension (2000), the declination (2000) and the b_J apparent magnitude, respectively, as reported in the COSMOS catalogue. Columns (4) and (5) give the heliocentric velocity ($v = cz$) and the internal error (in km/s). The external error can be derived by multiplying the error in column (5) by a factor of the order of 1.6 – 1.9: the lower value is obtained by comparing repeated observations of the same galaxies (Malumuth et al. 1992), while the higher one takes into account also the different reduction techniques (see the discussion in Bardelli et al. 1994). Finally, the code “emiss” in column (6) denotes the velocities determined from emission lines.

The galaxies whose spectrum presents detectable emission lines (mainly [OII] λ 3727, H β λ 4860, [OIII] λ 4959 and [OIII] λ 5007) are 133, corresponding to a percentage of 22%, significantly higher than the average value of 16% reported by Biviano et al. (1997) for the cluster galaxy population.

From the literature data, we added 30 galaxies from the ENACS survey (Katgert et al. 1998), 17 from Quintana et al. (1995) and 43 from the compilation of Fairall & Jones (1991): in case of multiple values for the same galaxy, we adopted the most recent estimate. The final sample contains a total of 671 velocities.

In Fig. 2 we plot the redshift completeness within the

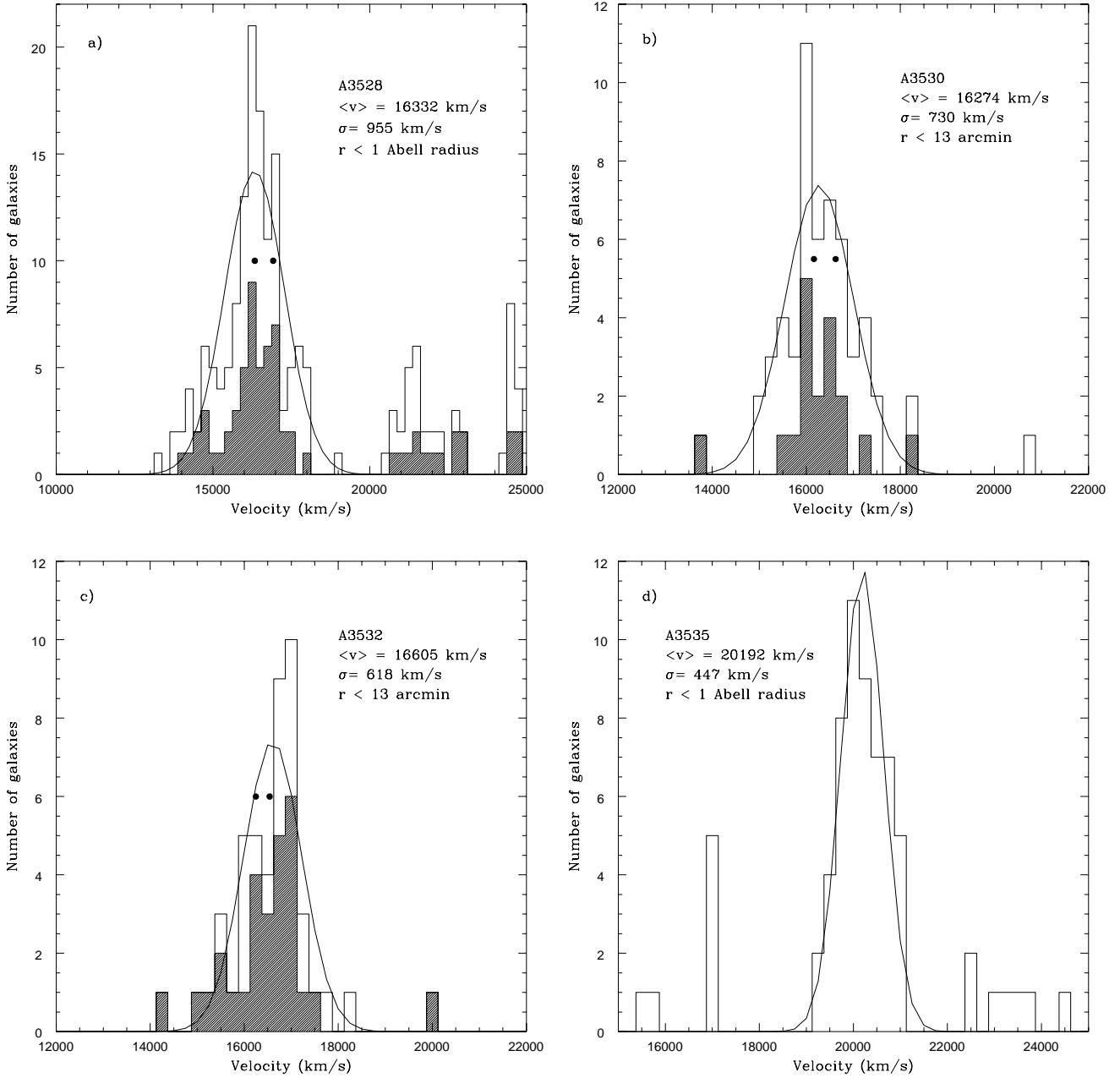


Figure 5. Velocity histograms for the four ACO clusters in the complex: a) A3528; b) A3530; c) A3532; d) A3535. A Gaussian with mean value $\langle v \rangle$ and dispersion σ has been superimposed on each distribution: the parameters for each cluster are reported in the labels. The shadowed histograms in the first three panels correspond to galaxies with $b_J < 18$.

OPTOPUS fields as a function of magnitude. The first bin includes all galaxies with $b_J < 16.5$. The differential completeness is higher than 70% for objects with $b_J < 18.5$: at this limit the integrated completeness is $\sim 83\%$.

In Fig. 3, the wedge diagram of the galaxies of our sample in the velocity range 11000 – 24000 km/s is reported. In this plot the right ascension coordinate has been compressed and the plotted coordinate is declination, in order to better visualize the structure, which is elongated in the North–South direction. Note that, in this representation, A3530 and A3532 appear compressed together. From this figure it

is clear the presence of the “finger-of-God” of the clusters and the physical connection between them. Note also the region without galaxies in the foreground of the structure.

In Fig. 4 the velocity histogram of our sample is shown: the main peak at ~ 16000 km/s corresponds to A3528, A3530 and A3532, while the peak at ~ 20000 km/s corresponds to A3535.

These data were used in Bardelli et al. (2000) to estimate the density excess of the A3528 complex with respect to a uniform distribution. We found $\frac{N}{N} = 21.4 \pm 1.2$ on a scale of $5.3 \text{ h}^{-1} \text{ Mpc}$, which corresponds to a mass of

$3.6 \times 10^{15} \Omega_o h^{-1} M_\odot$, under the hypothesis that light traces mass. Analyzing the galaxy density profile, we found a significant void in the foreground (at ~ 10000 km/s); in the background of the structure we detected a void at a mean velocity of ~ 35000 km/s and a significant overdensity at ~ 30000 km/s which is part of a larger structure (see the discussion in Bardelli et al. 2000).

4 DYNAMICAL PARAMETERS OF THE CLUSTERS

The basic parameters which describe the dynamics of a cluster are the mean velocity $\langle v \rangle$ and the velocity dispersion σ . In order to estimate these quantities we used the biweight location and scale estimators (Beers et al. 1990). The velocity range, in which the cluster members lie, is found by assuming that the velocity distribution is Gaussian and the procedure used for rejecting interlopers is described in Bardelli et al. (1994).

The parameters obtained for the clusters in the complex are reported in Table 3: column (1) and (2) give the cluster name and the number of galaxies used to estimate the dynamical parameters, column (4) and (5) show the mean velocity and the velocity dispersion (with their 1σ errors). For A3528 and A3535 we considered galaxies inside one Abell radius from the cluster center (i.e. $31'$ and $25'$ respectively); for A3530 and A3532, given the fact that their Abell circles overlap each other, we restricted our analysis to galaxies inside a circle of 13 arcmin radius. In Fig. 5 the velocity histograms for each cluster are shown, with superimposed a Gaussian with mean value $\langle v \rangle$ and dispersion σ ; the shaded histograms correspond to galaxies with $b_J < 18$.

Comparing our parameters reported in Table 3 with the literature values (see Sect. 2), we find significant differences. The velocity distribution of galaxies in A3528, although globally consistent with a single Gaussian, appears characterized by several peaks. In particular, considering the distribution of bright galaxies ($b_J < 18$, shadowed histogram in Fig. 5a) the presence of a bump at lower velocity (~ 14500 km/s) is clear. Given the fact that the ENACS and the Quintana et al. (1995) estimates are based on galaxies brighter than ~ 18 , this tail can explain their lower values for $\langle v \rangle$. An analogous justification can explain the differences for A3530 and A3532, in addition to the fact that for these two clusters we restricted the analysis to the very central regions. Finally, for A3535 the difference with the literature value is justified by the fact that the Vettolani et al. (1990) estimate was based only on 4 galaxies.

Another interesting characteristic of this complex is that all clusters appear dominated by a pair of bright ellipticals, instead of a single dominant galaxy. In particular, A3530 and A3532 are both dominated by a dumb-bell system (Gregorini et al. 1994), i.e. two galaxies of roughly equal brightness inside a common halo. Moreover, the major axes of these systems are both roughly aligned in the East–West direction, along the main axis of the cluster pair. In Fig. 5b and 5c, the black dots show the radial velocity of each components of these dumb-bell systems. It is interesting to note that these components are in correspondence of two separated peaks in the velocity distributions; however, it is not

Table 3. Dynamical parameters of clusters in the A3528 complex

Cluster	N_{gal}	$\langle v \rangle$ (km/s)	σ (km/s)	notes
A3528	135	16332^{+72}_{-116}	955^{+86}_{-86}	1 Abell radius
A3530	54	16274^{+78}_{-110}	730^{+143}_{-53}	13' radius
A3532	45	16605^{+76}_{-161}	618^{+158}_{-28}	13' radius
A3535	53	20192^{+78}_{-62}	447^{+42}_{-22}	1 Abell radius

Table 4. Groups in the bi–dimensional sample

#	α (2000)	δ (2000)	# mem.	notes
B792	12 53 32.6	-28 20 00	22	
B806	12 53 53.6	-28 34 25	50	A3528
B944	12 54 10.7	-29 00 05	68	A3528
B929	12 54 12.1	-28 44 56	27	A3528
B1014	12 54 27.7	-29 07 30	31	A3528
B1107	12 54 44.0	-29 17 30	17	A3528
B1181	12 54 50.6	-29 02 09	20	A3528
B1445	12 55 26.3	-29 24 09	29	A3528
B1420	12 55 35.5	-30 21 31	40	A3530
B1924	12 56 58.1	-30 28 58	44	A3532
B2011	12 57 17.6	-30 21 41	31	A3532
B2230	12 57 49.2	-28 30 27	43	A3535
B2282	12 57 52.8	-28 12 44	24	A3535

possible to assess at a high confidence level the significance of this bimodality (see below).

Also in the center of A3528 there are two bright galaxies, which are located near the positions of the two X-ray blobs observed by Schindler (1996), already discussed in Sect. 2. In Fig. 5a the radial velocities of these two galaxies are indicated by black dots: also in this case, there is a correspondence with two peaks in the velocity distribution.

For what concerns A3535, there is not a clear dominant galaxy near the center, although Gregorini et al. (1994) report the presence of a dumb-bell system.

In order to assess the statistical significance of the peaks in the velocity distribution, we applied the KMM test (Ashman, Bird & Zepf, 1994) which checks whether the distribution is better represented by a single or by a multiple Gaussian. Given the limited number of objects, the bimodality hypothesis is not significantly better than that of a single Gaussian for all clusters, even in the case of $b_J < 18$. However, the presence of these peaks leads to a marginal deviation from Gaussianity in A3528 (skewness test) and in A3530 (kurtosis test).

5 SUBSTRUCTURE ANALYSIS

The presence of substructures and their relevance in term of mass with respect to the main clusters are useful tools for

Table 5. Groups in the three-dimensional sample

#	α (2000)	δ (2000)	v_o (km/s)	# mem.	$\langle v \rangle$ (km/s)	σ (km/s)	notes
T362	12 54 36.6	-29 05 15	16223	111	16313^{+93}_{-76}	888^{+103}_{-82}	A3528
T352	12 54 57.3	-29 11 47	21354	21	21336^{+115}_{-84}	454^{+85}_{-86}	A3528
T460	12 55 12.8	-30 22 35	16322	78	16186^{+61}_{-97}	637^{+51}_{-38}	A3530
T443	12 56 08.0	-29 57 13	16748	27	16914^{+78}_{-84}	375^{+77}_{-40}	A3530/A3532
T342	12 56 19.6	-30 47 42	15891	17	15852^{+100}_{-290}	511^{+83}_{-84}	A3530/A3532
T331	12 56 32.6	-31 16 24	16679	41	16657^{+84}_{-138}	665^{+143}_{-47}	
T498	12 57 07.4	-30 23 29	16551	48	16646^{+56}_{-162}	612^{+93}_{-82}	A3532
T421	12 57 51.5	-28 31 53	20315	53	20239^{+71}_{-78}	455^{+35}_{-45}	A3535

understanding if a structure is relaxed. In order to detect subcomponents, we have used the DEDICA method (Algorithm driven by the density estimate for the identification of clusters, Pisani 1993, 1996), already applied by Bardelli et al. (1998b) to the A3558 cluster complex. The basic idea of this algorithm is to determine the density field $f(\vec{x})$ (where \vec{x} is the n -dimensional position vector) by smoothing the distribution of galaxy with a Gaussian adaptive kernel: the $f(\vec{x})$ is then represented as a sum of Gaussians, whose widths are dependent on the local density. Groups are found as local maxima of $f(\vec{x})$, while a likelihood function is constructed to estimate the confidence of the existence of the substructures (see for details Pisani 1993, 1996). As done in Bardelli et al. (1998b), we performed the analysis both in the bi-dimensional and three-dimensional samples: the first case, having more objects, does not suffer by small numbers statistic but could be biased by projection effects; the second case, although using a much smaller sample, is able to separate in velocity the clumps along the line of sight.

5.1 The bi-dimensional sample

The bi-dimensional sample is obtained by using the rectangular region described in Sect. 2, which contains 3048 galaxies brighter than $b_J = 19.5$. As done in Bardelli et al. (1998b), we estimated the background density by plotting the histogram of the widths σ of the Gaussians, which is a symmetric distribution with a tail at high σ . We define the value of the width of the background (σ_{bck}) as the value at the beginning of the tail, resulting in $\sigma_{bck} = 3.85$, corresponding to a density of $0.024 \text{ gal arcmin}^{-2}$. The whole range of densities in our sample is $0.015\text{--}1.587 \text{ gal arcmin}^{-2}$. The adopted χ^2 threshold is 14.0, corresponding to a significance of 99.99%.

The 13 significant groups found in our bi-dimensional sample are reported in Table 4, where column (1) is the identification number and columns (2) and (3) give the α and δ coordinates of the group center. These coordinates are identified as the common \vec{x}_{lim} positions of the members and they do not necessarily coincide with the geometrical center. Column (4) reports the number of the substructure

members and column (5) indicates the main component to which the substructure belongs. Note that this association has been made on the basis of a simple coincidence on the plane of the sky.

In Fig. 6 the positions of the substructure members are shown, superimposed on the isodensity contours of galaxies. Note that in these figures the isodensity contours are obtained directly by binning the data (see details in Sect. 3) and not from the \hat{f}_k : however the two methods give similar contours. Note that the objects displayed in Fig. 6 are the galaxies which resulted significantly assigned to the subclumps by our algorithm, but it is possible that the effective number of members of each group is higher.

The bi-dimensional analysis revealed that the A3528 complex is significantly substructured, with the presence of two or more clumps in the inner part of the single clusters (with the exception of A3530). In particular, it is interesting to note the series of clumps around A3528, aligned along the direction pointing toward A3530-A3532. The two X-ray blobs A3528N and A3528S are identified with B944 and B1107, respectively, at a separation of $\sim 2.5 \text{ arcmin}$ and $\sim 3.9 \text{ arcmin}$. The two dominant galaxies of A3528 (see Sect. 4) are located one in B944 and the other in B1107.

5.2 The three-dimensional sample

In this case we used the velocity sample described in Sect. 2: from the 671 galaxies with measured redshift we selected the 498 objects in the velocity range $[10000 - 22500] \text{ km/s}$.

Our formalism uses symmetric three-dimensional Gaussian kernels, with $\sigma_x = \sigma_y = \sigma_v$, and therefore it is necessary to scale the velocity interval in order to have a numerical range comparable to the other two variables: we have chosen to compress the velocity by a factor 100 (see Bardelli et al. 1998b for details about this point).

The adopted value of the background is $\sigma_{bck} = 10.0 \text{ arcmin}$, corresponding to $3.6 \times 10^{-4} \text{ gal arcmin}^{-2} (\text{km/s}/100)^{-1}$ and a significance threshold of $\chi^2 = 15.8$. The significant 3-D clusters are 8, out of a total of 19, and are reported in Table 5. Column (1) is the subcluster identification number, columns (2), (3) and (4) report the coordinates (α ,

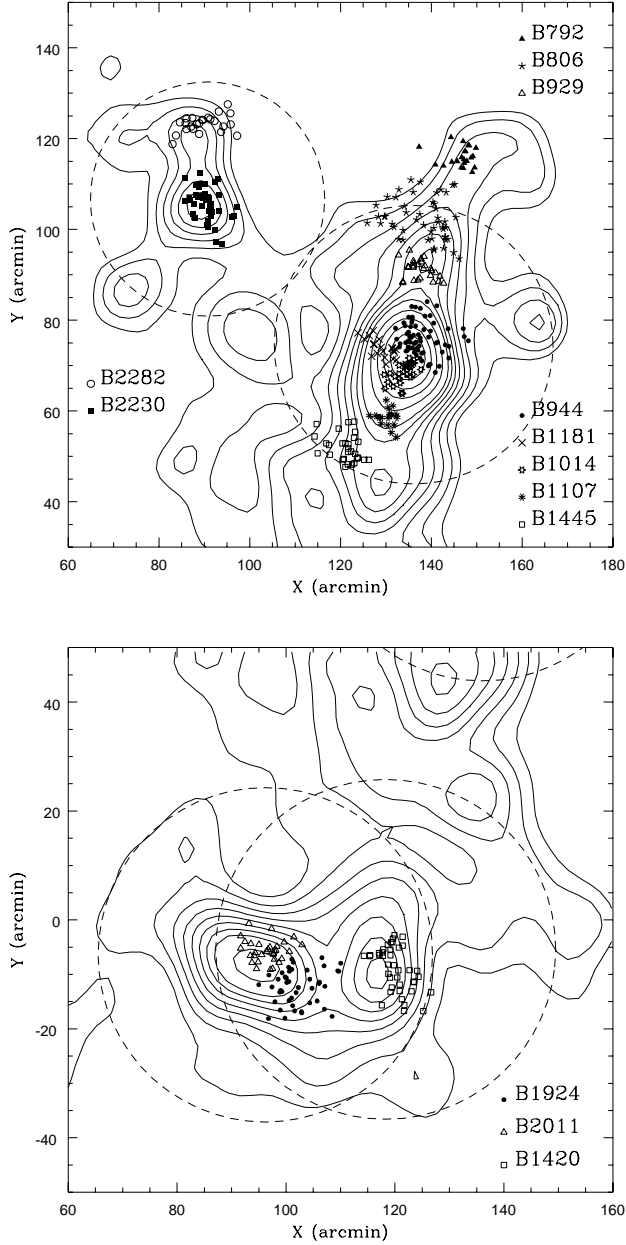


Figure 6. Groups in the A3528 region found in the bi-dimensional sample. The positions of subcluster galaxies are overplotted to the 2-D isodensity contours. Symbols used to label the different groups are explained in the figure. Upper panel: A3535 and A3528. Lower panel: A3532 and A3530.

δ and v_o) of the group center, while the number of members is reported in column (5). The estimated dynamical parameters are reported in columns (6) and (7) and in column (8) the association to the clusters of the structure is given. Also in this case, the association has been made on the basis of a simple coincidence on the plane of the sky. Note that v_o is the projection of \vec{x}_{lim} on the velocity axis, and therefore it does not necessarily coincide with $\langle v \rangle$.

In Fig. 7 the members of these groups are plotted: solid lines connect the position of each galaxy to the common limiting position \vec{x}_{lim} of the group. In the upper panel, the

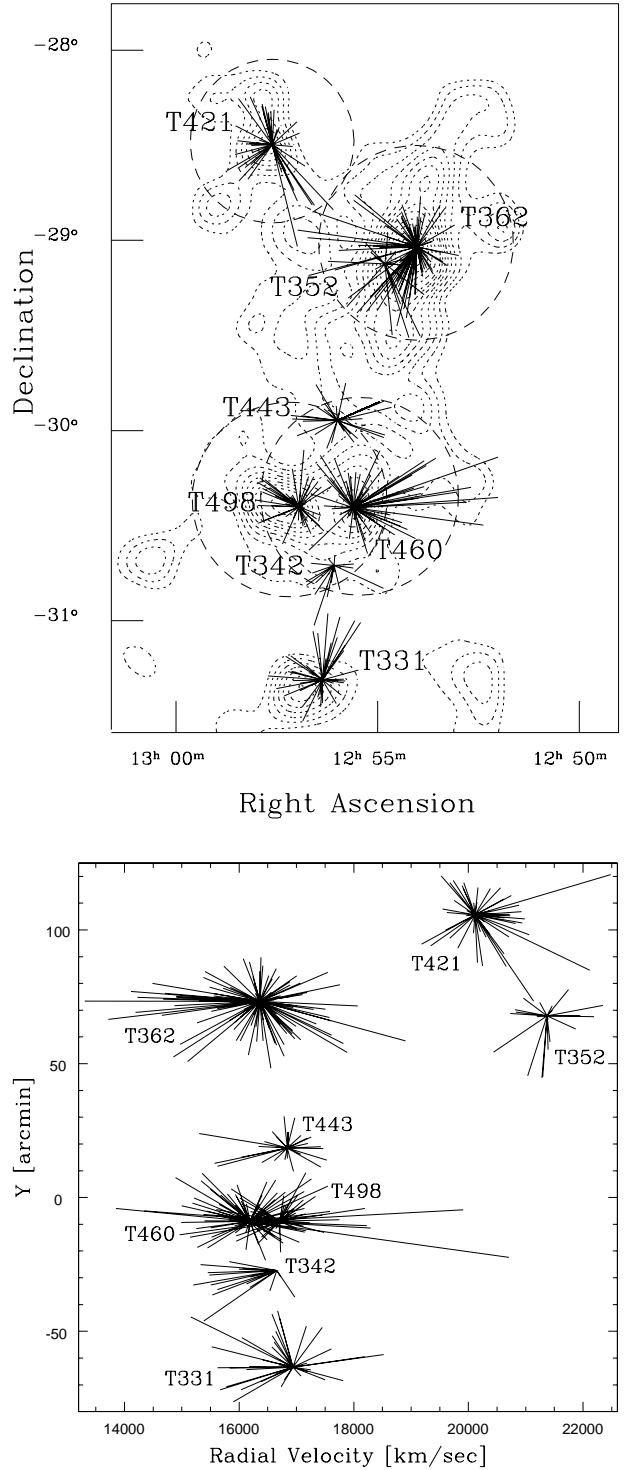


Figure 7. Groups in the A3528 region found in the three-dimensional sample. Solid lines connect the position of each galaxy to the common limiting position \vec{x}_{lim} of the group. Upper panel: projection on the plane of the sky. Lower panel: projection on the velocity-Y plane.

groups are projected on the plane of the sky, while in the lower panel they are shown in the velocity–Y plane in order to clarify the separation in velocity.

In this case, the sparse sampling introduced by the redshift survey with respect to the bi-dimensional sample leads to the loss of some substructures. In particular, only the A3528 cluster remains bimodal, with the main component at 16313 km/s (T362) and a secondary clump at 21336 km/s (T352).

6 DISCUSSION

The A3528 cluster complex is located in a region of enhanced dynamical activity, where clusters are accreting matter in a series of spectacular mergings, as seen in the nearby system dominated by A3558 (see Bardelli et al. 1998b). However, these two cluster complexes show some relevant differences.

In the A3558 complex, the members of the chain appeared to be fragmented in a large number of components, both in optical and in X-ray band. In fact, from the optical substructure analysis we found 21 significant three-dimensional subclumps; in the X-ray band, in addition to the three ACO clusters A3558, A3562 and A3556, also two poor groups (SC1329-313 and SC1327-312) were detected. All these components are embedded in a hot gas filament (Bardelli et al. 1996; Kull & Böhringer 1999). Moreover, Venturi et al. (2000) found a deficiency of radiogalaxies in the A3558 complex with respect to the radio–optical luminosity function of normal clusters and Bardelli et al. (1998b) found an excess of blue galaxies in the expected position of the shock.

These facts could suggest that the dynamical processes acting on this complex are in a rather advanced stage and that the merging events were already able to induce modifications in the galaxy population. Our conclusion is that the A3558 complex is a cluster-cluster collision (otherwise called “major merging”) seen just after the first core-core encounter, where an intervening cluster impacted onto the richer object A3558. Indeed the clumpiness found eastward of A3558 could be due to the galaxies of this intervening cluster, which is now emerging from the main component. This scenario is also confirmed by numerical simulations of merging clusters (see f.i. lower panels in Fig.2 of Burns et al. 1994, which show the structure after the core-core encounter).

The A3528 complex is characterized in the X-ray band (ROSAT pointed observations) by two pairs of roughly similar interacting clumps: one pair has been resolved as two optical clusters (A3530 and A3532), while the two components of the other pair are both associated to A3528. The radio–optical luminosity function of the radiogalaxies in this complex does not appear significantly different from that of normal clusters (Venturi et al., in preparation).

From the analysis of optical data, we find that the velocity histograms of cluster galaxies are not significantly different from a Gaussian distribution, meaning that the inner parts of the clusters are not far from the virial equilibrium. However, from our substructure analysis the A3528 complex appears characterized by a number of subclumps. In particular, it is interesting to note in the bi-dimensional sample the series of clumps around A3528, aligned along the direction pointing toward A3530-A3532. Moreover, two

of them appear associated with A3528N and A3528S (B944 and B1107, respectively). The association is based not only on the $\alpha - \delta$ positional coincidence, but also on the mean velocity concordance: in fact, for each group the mode of the velocity distribution of members with redshift is in agreement with the velocity of the dominant galaxy of the corresponding X-ray blob. Also in the three-dimensional sample A3528 appears formed by two groups, T362 and T352, but while the first is located at $\langle v \rangle = 16313$ km/s, the second has $\langle v \rangle = 21336$ km/s, i.e. it is placed in the background of the cluster. In fact, it results that most members of B944 and B1107 are part of the same three-dimensional clump (T352). This link of some bi-dimensional groups into a single three-dimensional clump happens also for other substructures and is due to the sparse sampling introduced by the redshift survey, which in some cases does not allow a statistically significant separation of the subcomponents.

For what concerns the A3530-A3532 pair, the most puzzling feature is the presence of two dumb-bell galaxies at their centers, elongated along the axis joining the two clusters (see Sect. 4). Moreover, it is interesting to note the presence of two subclumps (T443 and T342) at the intersection of the Abell radii of the clusters, with mean velocity in agreement with the main components.

However, the A3528 complex is less fragmented than the A3558 structure: in fact, even if these two complexes have similar sizes, in the A3528 complex we detect only 8 significant three-dimensional subclumps against the 21 detected in the A3558 complex (see above).

All these characteristics of the A3528 complex seem to indicate that this is a “young” structure: the two interacting cluster pairs (A3528N-A3528S and A3530-A3532) resemble the simulations of Burns et al. (1994) for the pre-merger case (see upper panels of their Fig.2). This scenario is consistent with the suggestions of Reid et al. (1998), based on the analysis of extended radiosources in this region and with the fact that the merging effects on the galaxy population and on the cluster dynamics are not yet evident.

Given the overall overdensity of this region, at the end these two main components will merge together in a major merging event, forming a structure similar to the A3558 complex. The “age” difference of the two complexes is mainly due to their overdensities, which lead to different collapse times (see Table 5 in Bardelli et al. 2000). This fact confirms that the Shapley Concentration is a “laboratory” where it is possible to study the formation of clusters at different stages.

A better understanding of the status of the merging process in the A3528 complex will be reached using XMM observations of all clusters in the complex (AO1 approved observations), which will allow us to derive the distribution of the diffuse hot gas and its temperature map, leading to estimate the cluster masses and to individuate the position of the shock fronts.

Finally, a more detailed analysis of the galaxy population properties will be possible through the spectral classification of galaxies in the two cluster complexes and in the underlying supercluster “field” (Baldi et al., in preparation). This study will help to understand the effects of the cluster large-scale dynamics on the galaxy morphology.

ACKNOWLEDGEMENTS

We warmly thank T.C.Beers, C.M.Bird and A.Pisani for having distributed public versions of their programmes (RO-STAT, KMM and DEDICA). We also thank the referee (M.Drinkwater) for useful comments which improved the presentation of the results.

REFERENCES

- Abell G.O., Corwin H.G., Olowin R.P., 1989, *ApJSS* 70, 1
 Ashman K.M., Bird C.M., Zepf S.E., 1994, *AJ* 108, 2348
 Bardelli S., Zucca E., Vettolani G., Zamorani G., Scaramella R., Collins C.A., MacGillivray H.T., 1994, *MNRAS* 267, 665
 Bardelli S., Zucca E., Malizia A., Zamorani G., Scaramella R., Vettolani G., 1996, *A&A* 305, 435
 Bardelli S., Zucca E., Zamorani G., Vettolani G., Scaramella R., 1998a, *MNRAS* 296, 599
 Bardelli S., Pisani A., Ramella M., Zucca E., Zamorani G., 1998b, *MNRAS* 300, 589
 Bardelli S., Zucca E., Zamorani G., Moscardini L., Scaramella R., 2000, *MNRAS* 312, 540
 Beers T.C., Flynn K., Gebhardt K., 1990, *AJ* 100, 32
 Bird C.M., 1994, *AJ* 107, 1637
 Biviano A., Katgert P., Mazure A., Moles M., den Hartog R., Perea J., Focardi P., 1997, *A&A* 321, 84
 Burns J.O., Roettiger K., Ledlow M., Klypin A., 1994, *ApJL* 427, L87
 Colberg J.M., White S.D.M., Jenkins A., Pearce F.R., 1998, *MNRAS* 308, 593
 Ettori S., Fabian A.C., White D.A., 1997, *MNRAS* 289, 787
 Ettori S., Bardelli S., De Grandi S., Molendi S., Zamorani G., Zucca E., 2000, *MNRAS* in press (astro-ph 0006014)
 Fairall A.P., Jones A., 1991, *Southern Redshifts Catalogue and Plots*, Publ. Dept. of Astronomy, Univ. Cape Town, No. 11
 Gregorini L., de Ruiter H.R., Parma P., Sadler E.M., Vettolani G., Ekers R.D., 1994, *A&ASS* 106, 1
 Henriksen M., Jones C., 1996 *ApJ* 465, 666
 Katgert P., Mazure A., den Hartog R., Adami C., Biviano A., Perea J., 1998, *A&ASS* 129, 399
 Kull A., Böhringer H., 1999, *A&A* 341, 23
 Kurtz M.J., Mink D.J., Wyatt W.F., Fabricant D.G., Torres G., Kriss G.A., Tonry J.L., 1992, in Worrall D.M., Biemesderfer C., Barnes J. eds, *Astronomical Data Analysis Software and Systems I*, ASP conference series vol.25, p.432
 Lund G., 1986, *OPTOPUS - ESO Operating Manual No. 6*
 Malumuth E.M., Kriss G.A., Van Dyke Dixon W., Ferguson H.C., Ritchie C., 1992, *AJ* 104, 495
 Mazure A. et al., 1996, *A&A* 310, 31
 Pisani A., 1993, *MNRAS* 265, 706
 Pisani A., 1996, *MNRAS* 278, 697
 Quintana H., Ramirez A., Melnick J., Raychaudhury S., Szelak E., 1995, *AJ* 110, 463
 Reid A.D., Hunstead R.W., Pierre M.M., 1998, *MNRAS* 296, 949
 Schindler S., 1996 *MNRAS* 280, 309
 Venturi T., Bardelli S., Morganti R., Hunstead R.W., 1997, *MNRAS* 285, 898
 Venturi T., Bardelli S., Morganti R., Hunstead R.W., 1998a, *MNRAS* 298, 1113
 Venturi T., Bardelli S., Dallacasa D., Morganti R., Hunstead R.W., 1998b, in G. Giuricin, M. Mezzetti & P. Salucci eds, *Observational Cosmology: the development of galaxy systems*, ASP Conf. Ser. Vol. 176, p. 256
 Venturi T., Bardelli S., Morganti R., Hunstead R.W., 2000, *MNRAS* 314, 594
 Vettolani G., Chincarini G., Scaramella R., Zamorani G., 1990 *AJ* 99, 1709
 White D.A., Jones C., Forman W., 1997, *MNRAS* 292, 419
 Wyse R.F., Gilmore G., 1992, *MNRAS* 257, 1
 Yentis D.J., Cruddace R.G., Gursky H., Stuart B.V., Wallin J.F., MacGillivray H.T., Collins C.A., 1992, in MacGillivray H.T., Collins C.A. eds, *Digitized Optical Sky Surveys*, Kluwer, Dordrecht, p.67
 Zucca E., Zamorani G., Scaramella R., Vettolani G., 1993, *ApJ* 407, 470

Table 2. Redshift data for the A3528 complex sample

α (2000)	δ (2000)	b_J	v (km/s)	err	notes
12 51 18.66	-30 19 02.7	14.98	4564	28	
12 51 19.41	-30 25 42.7	18.80	31465	63	
12 51 23.97	-30 18 04.1	15.87	4579	61	emiss
12 51 27.13	-30 10 56.0	17.76	19390	15	emiss
12 51 27.89	-30 19 00.1	18.56	27564	51	
12 51 39.32	-30 17 10.8	17.94	27326	46	
12 51 40.76	-30 27 05.8	18.80	31584	79	emiss
12 51 46.79	-28 23 20.5	17.29	15854	57	
12 51 50.56	-28 23 35.7	17.29	25999	42	emiss
12 51 52.01	-28 18 55.3	18.69	25735	95	emiss
12 52 01.51	-30 10 46.7	18.73	20274	116	emiss
12 52 02.43	-28 23 40.9	17.48	15705	30	
12 52 09.63	-28 32 25.7	17.22	16995	32	
12 52 09.63	-28 13 30.5	17.29	21211	81	
12 52 12.90	-28 20 18.7	18.20	29812	37	
12 52 13.37	-30 19 49.6	17.62	16042	104	
12 52 15.12	-30 07 06.9	16.87	17264	36	
12 52 19.74	-30 30 20.0	17.90	31572	68	emiss
12 52 31.14	-28 23 24.1	17.71	14806	36	
12 52 32.40	-28 12 27.0	18.77	54096	15	emiss
12 52 32.98	-28 27 14.5	17.90	17032	56	
12 52 33.71	-30 28 38.7	18.89	16618	15	emiss
12 52 33.92	-30 26 52.1	18.97	60325	69	
12 52 34.43	-30 14 51.3	17.58	27457	15	emiss
12 52 35.82	-30 08 16.8	18.86	54163	92	
12 52 36.51	-28 25 25.9	18.69	29047	64	emiss
12 52 40.05	-28 23 38.2	18.78	14844	38	
12 52 43.40	-30 24 01.3	18.47	32472	67	
12 52 45.21	-30 35 38.9	18.99	21475	15	emiss
12 52 46.33	-28 36 13.6	17.73	14886	45	
12 52 46.37	-30 13 36.5	17.08	20949	34	
12 52 46.40	-30 28 06.3	18.18	32571	68	
12 52 46.95	-30 32 57.6	18.66	31832	49	
12 52 47.63	-30 16 40.7	18.03	31450	48	
12 52 48.32	-30 06 51.4	18.49	27398	15	emiss
12 52 49.02	-28 15 29.9	18.70	50037	60	emiss
12 52 49.37	-30 30 18.1	18.32	31372	54	
12 52 51.30	-30 14 59.3	18.80	31876	95	emiss
12 52 51.59	-30 26 59.9	18.76	31911	58	
12 52 53.09	-30 16 52.5	19.01	15650	15	emiss
12 52 56.46	-29 48 28.1	16.73	15057	45	
12 52 58.99	-30 21 35.2	17.73	15739	57	
12 53 00.05	-30 09 13.3	18.89	25956	44	
12 53 00.90	-28 36 51.6	18.11	16716	107	
12 53 04.40	-30 23 54.3	18.62	50143	81	emiss
12 53 05.03	-28 07 42.0	17.46	3042	15	emiss
12 53 06.53	-30 16 33.2	18.77	31783	51	
12 53 08.28	-30 01 14.8	18.34	27931	94	emiss
12 53 12.70	-28 28 55.6	18.24	16469	30	
12 53 13.28	-30 18 29.8	17.62	17138	43	
12 53 13.58	-28 25 47.4	18.38	17269	81	
12 53 15.28	-28 32 41.2	18.68	15795	96	emiss
12 53 16.20	-29 08 46.6	18.71	41256	81	
12 53 17.46	-29 46 09.4	17.48	15086	56	
12 53 17.72	-30 24 38.2	18.94	32039	58	
12 53 17.79	-28 30 58.5	18.18	25612	119	emiss
12 53 19.12	-30 30 19.3	17.97	30917	36	
12 53 19.19	-29 03 49.0	18.10	16515	79	
12 53 19.91	-30 26 58.2	17.75	30657	63	emiss
12 53 20.25	-28 25 50.7	18.19	18555	15	emiss
12 53 21.23	-30 18 55.4	18.32	44359	68	
12 53 22.87	-28 16 24.5	18.38	17689	15	emiss
12 53 23.69	-28 20 45.5	17.00	16415	59	emiss

Table 2. cont.

α (2000)	δ (2000)	b_J	v (km/s)	err	notes
12 53 24.18	-28 28 47.0	16.02	8086	28	
12 53 25.54	-28 18 18.3	18.20	16287	15	emiss
12 53 26.02	-28 54 11.4	17.84	16265	69	
12 53 26.81	-30 07 04.5	18.40	25871	62	
12 53 27.40	-28 18 36.6	17.78	33257	105	emiss
12 53 29.81	-28 09 21.7	18.38	28874	15	emiss
12 53 30.69	-28 15 52.6	17.15	16705	29	
12 53 30.82	-28 11 29.2	18.21	16988	15	emiss
12 53 34.04	-30 03 21.4	18.79	41747	15	emiss
12 53 34.42	-28 19 48.2	16.31	16281	40	
12 53 34.59	-28 18 58.2	18.60	16717	38	
12 53 35.25	-29 07 04.9	18.52	16016	50	
12 53 35.77	-28 15 01.0	17.15	16330	15	emiss
12 53 38.28	-29 48 11.2	18.25	21069	15	emiss
12 53 39.82	-30 04 36.6	18.72	21413	15	emiss
12 53 40.06	-29 38 51.9	18.14	25854	82	emiss
12 53 40.49	-28 48 57.9	17.06	16649	73	
12 53 41.24	-28 19 27.4	18.37	21029	70	emiss
12 53 41.26	-29 05 52.8	18.49	16566	59	
12 53 41.37	-29 50 34.3	18.21	20962	83	emiss
12 53 45.67	-30 07 58.7	17.53	16640	58	
12 53 47.52	-28 48 02.4	18.82	15736	49	emiss
12 53 47.95	-28 14 11.9	17.96	15586	38	
12 53 48.17	-29 45 43.3	18.89	31033	15	emiss
12 53 48.20	-30 00 00.7	18.40	20559	35	
12 53 48.43	-30 22 25.6	19.03	31913	31	
12 53 50.29	-30 00 23.6	17.72	20589	41	
12 53 50.85	-29 46 17.0	18.86	30917	15	emiss
12 53 53.51	-29 47 14.1	18.61	30731	82	emiss
12 53 54.97	-28 20 28.8	17.44	15679	29	
12 53 55.22	-29 09 51.3	18.80	16716	69	
12 53 55.27	-30 06 48.5	18.38	26007	34	
12 53 57.03	-28 59 25.8	18.53	16493	112	emiss
12 53 57.06	-28 25 46.7	18.65	18030	171	
12 53 57.10	-29 08 29.9	18.42	17606	36	emiss
12 53 57.49	-30 22 39.3	18.48	21633	43	
12 53 57.89	-29 51 46.4	17.92	27888	31	
12 53 58.54	-28 59 37.5	18.00	15833	38	
12 53 58.65	-29 06 05.5	18.84	16654	56	
12 53 59.03	-30 10 21.0	19.12	17546	61	
12 54 00.50	-29 53 58.9	18.73	27838	88	
12 54 01.64	-29 49 06.8	18.57	27762	73	
12 54 01.75	-30 16 58.5	18.95	16354	80	
12 54 02.55	-30 08 48.0	18.59	16483	31	
12 54 02.66	-30 18 46.5	19.19	20786	37	
12 54 03.82	-29 31 13.6	18.21	17018	38	
12 54 04.68	-29 08 04.0	18.87	13720	85	
12 54 05.77	-30 19 08.4	18.12	16962	45	
12 54 06.21	-28 58 19.0	19.34	16283	92	
12 54 06.55	-30 08 46.3	18.61	32535	105	
12 54 06.93	-29 50 44.6	18.13	21029	15	emiss
12 54 07.59	-29 16 27.8	18.02	21424	71	
12 54 07.97	-29 08 23.1	18.51	16421	58	
12 54 08.46	-28 50 31.5	17.93	17546	62	
12 54 08.69	-29 47 51.9	17.16	21025	32	
12 54 09.79	-30 20 42.2	17.49	16046	53	
12 54 09.86	-30 16 09.0	19.03	46420	75	emiss
12 54 12.02	-29 29 31.4	19.24	21296	10	emiss
12 54 12.05	-29 09 22.7	17.64	15910	36	
12 54 12.36	-29 32 30.7	18.78	44170	93	
12 54 12.60	-29 03 37.5	18.57	16945	38	
12 54 12.76	-29 58 29.7	18.94	31862	42	
12 54 12.80	-29 53 04.6	18.04	21495	31	

Table 2. cont.

α (2000)	δ (2000)	b_J	v (km/s)	err	notes
12 54 12.80	-30 33 21.8	16.82	15271	35	
12 54 13.27	-29 05 30.7	18.86	14192	57	
12 54 14.35	-29 03 02.5	18.10	18069	111	
12 54 15.08	-28 52 02.9	18.66	16706	57	
12 54 15.13	-29 49 00.1	17.36	20862	27	
12 54 16.36	-29 47 35.8	18.57	27605	72	emiss
12 54 16.39	-30 17 28.5	18.06	15929	72	
12 54 16.78	-29 01 17.4	18.23	15310	39	
12 54 17.36	-29 31 03.1	16.96	24727	34	
12 54 17.46	-29 00 48.4	18.45	16359	51	
12 54 18.94	-28 59 30.3	18.36	14898	87	
12 54 19.17	-30 14 41.1	19.01	31726	91	emiss
12 54 19.55	-29 01 20.0	18.73	16112	47	
12 54 19.72	-30 13 25.3	18.01	15795	41	
12 54 19.99	-29 27 40.8	18.84	24422	42	
12 54 20.09	-28 51 47.0	18.39	16515	41	
12 54 20.28	-29 04 08.1	16.88	16521	74	
12 54 20.36	-29 01 47.1	18.09	21244	98	
12 54 20.38	-29 16 27.2	18.42	16307	60	
12 54 20.40	-29 48 40.0	17.92	20828	60	
12 54 20.94	-29 06 37.6	18.60	14653	52	
12 54 21.21	-29 16 02.4	18.55	15951	59	
12 54 21.52	-28 58 00.0	18.76	16564	52	
12 54 23.13	-29 46 19.9	18.96	31914	77	
12 54 23.43	-29 05 04.0	17.03	15514	59	
12 54 23.48	-29 10 02.2	17.75	16518	38	
12 54 23.50	-28 55 10.6	18.76	17758	50	
12 54 23.70	-29 20 03.8	19.10	24521	92	
12 54 24.02	-29 34 59.0	19.12	15040	100	
12 54 24.43	-30 15 07.4	18.57	31759	54	
12 54 24.62	-28 56 07.6	18.73	15848	52	
12 54 24.86	-30 30 36.3	16.77	16742	37	
12 54 24.99	-29 04 41.1	18.33	21468	51	
12 54 25.31	-29 03 03.4	18.10	17011	49	
12 54 25.59	-29 29 21.6	17.89	28420	55	
12 54 26.60	-29 00 36.5	18.19	15869	56	
12 54 26.63	-28 59 20.9	18.64	15556	54	
12 54 26.71	-28 54 02.1	18.85	16887	63	
12 54 28.77	-29 30 00.4	17.98	21282	15	emiss
12 54 28.79	-29 17 31.4	17.29	14969	45	
12 54 29.54	-29 04 26.3	18.92	16087	57	
12 54 31.46	-28 55 18.8	17.56	16892	45	
12 54 31.47	-29 10 56.8	18.77	16290	54	
12 54 32.38	-29 26 05.3	18.85	28167	15	emiss
12 54 32.97	-29 23 53.0	19.07	15100	48	
12 54 33.03	-30 28 30.6	19.01	16589	50	
12 54 33.16	-28 46 29.5	18.68	55142	49	
12 54 33.80	-29 08 35.3	17.24	15835	49	
12 54 34.67	-29 59 16.6	18.11	23000	73	emiss
12 54 34.71	-28 59 54.3	18.49	14224	42	
12 54 34.77	-29 23 02.9	19.23	25953	44	
12 54 35.01	-30 29 39.9	17.83	15517	48	emiss
12 54 35.02	-29 07 29.2	18.80	17577	60	
12 54 35.46	-29 38 19.4	18.57	42043	39	
12 54 36.39	-29 16 12.8	19.17	16418	42	
12 54 36.48	-28 51 25.7	18.50	40883	56	
12 54 36.55	-29 20 33.5	18.14	17885	35	
12 54 38.10	-29 39 00.2	18.80	17626	56	
12 54 38.31	-30 09 19.6	17.94	4999	13	emiss
12 54 38.76	-30 13 50.8	17.82	15676	15	emiss
12 54 38.92	-29 01 10.6	18.21	15642	56	
12 54 39.26	-29 17 51.5	19.14	16655	48	
12 54 40.25	-29 43 52.8	18.60	16069	42	

Table 2. cont.

α (2000)	δ (2000)	b_J	v (km/s)	err	notes
12 54 40.91	-28 53 01.6	17.28	16576	33	
12 54 40.96	-29 01 23.5	18.91	13307	72	
12 54 41.84	-29 19 33.1	18.33	21393	16	emiss
12 54 42.34	-28 48 07.4	18.65	16413	53	
12 54 42.41	-28 51 55.0	17.48	17003	53	
12 54 43.00	-28 52 15.1	17.03	16242	42	
12 54 43.12	-28 50 15.9	17.67	16359	50	
12 54 43.26	-29 15 51.7	18.61	13802	55	
12 54 43.39	-29 15 25.5	18.62	16971	57	
12 54 43.40	-30 32 21.8	18.13	16340	33	
12 54 43.83	-29 30 38.8	18.84	24324	40	
12 54 44.24	-29 36 58.6	18.47	15130	132	
12 54 44.26	-29 06 30.2	18.34	16063	43	
12 54 45.00	-29 31 09.3	19.07	32275	106	
12 54 45.52	-29 14 06.2	18.52	17612	48	
12 54 45.52	-29 16 15.7	18.96	16022	35	
12 54 45.65	-29 17 54.8	18.21	13951	33	
12 54 46.11	-29 29 23.3	18.38	16269	27	
12 54 46.29	-29 26 28.8	18.99	16554	32	
12 54 47.59	-29 12 25.7	18.07	16934	52	
12 54 48.04	-30 16 56.6	19.25	15184	45	
12 54 49.30	-30 19 34.1	17.87	16081	34	
12 54 49.68	-28 52 35.5	18.77	15377	51	
12 54 50.08	-29 03 01.8	18.22	22345	106	
12 54 50.39	-30 26 08.8	19.10	16865	26	
12 54 51.70	-29 52 11.2	17.97	17259	34	
12 54 52.24	-29 17 37.8	18.17	14371	34	
12 54 52.68	-29 29 22.0	18.27	21035	106	
12 54 53.60	-29 34 43.9	17.30	16353	35	
12 54 53.81	-30 16 11.0	18.88	16039	68	
12 54 53.81	-29 00 46.6	17.46	16140	36	
12 54 54.71	-29 16 16.0	18.92	18902	30	
12 54 54.83	-30 21 34.0	19.02	15586	46	
12 54 55.33	-29 30 12.2	17.52	16324	37	
12 54 55.41	-28 54 17.0	17.15	22905	51	
12 54 56.65	-29 50 10.2	17.45	14860	94	emiss
12 54 57.01	-29 11 54.3	18.11	21872	33	
12 54 57.69	-30 30 40.9	19.24	16488	44	
12 54 57.85	-29 15 55.7	19.10	14746	107	
12 54 58.14	-30 13 43.6	18.22	25943	81	
12 54 58.40	-30 49 18.6	18.53	15622	55	
12 54 58.51	-29 41 44.5	18.33	17734	172	
12 55 00.18	-29 11 33.0	18.64	16526	67	
12 55 00.41	-30 00 56.0	18.64	17528	35	
12 55 00.54	-29 07 15.1	18.49	21193	54	
12 55 00.97	-29 00 05.0	18.31	14906	139	
12 55 01.04	-30 43 37.9	17.69	42778	61	emiss
12 55 01.19	-29 47 20.7	17.38	20802	84	emiss
12 55 02.05	-28 57 10.6	17.47	21747	57	
12 55 02.12	-30 08 43.7	18.33	20723	86	
12 55 02.26	-30 01 47.3	18.72	16395	28	
12 55 02.39	-29 28 59.1	18.39	17692	45	
12 55 02.87	-29 50 18.8	18.77	16576	81	
12 55 03.16	-29 38 52.0	17.91	24603	41	
12 55 03.30	-30 11 50.0	17.52	15498	54	
12 55 04.06	-29 15 54.5	17.96	17076	37	
12 55 04.10	-29 25 37.5	17.82	28989	27	
12 55 04.96	-29 08 24.4	18.89	21393	52	emiss
12 55 05.87	-28 58 15.9	18.18	17186	87	
12 55 06.22	-28 54 43.4	18.27	17065	162	
12 55 07.29	-30 05 52.8	17.49	15355	93	emiss
12 55 07.41	-29 31 33.0	18.02	24741	46	
12 55 07.87	-29 29 44.8	17.92	17103	35	

Table 2. cont.

α (2000)	δ (2000)	b_J	v (km/s)	err	notes
12 55 08.09	-30 45 06.4	18.52	16517	32	
12 55 08.38	-30 43 25.0	16.35	17709	24	
12 55 09.61	-29 50 31.9	18.08	16857	35	
12 55 09.72	-29 30 54.2	18.52	15163	50	
12 55 11.36	-30 26 23.2	18.01	16034	48	
12 55 13.07	-30 47 19.8	18.86	49439	15	emiss
12 55 13.18	-29 40 37.1	17.84	15671	46	
12 55 13.20	-30 28 02.1	17.76	16112	47	
12 55 13.73	-29 01 48.3	18.72	15903	53	
12 55 14.64	-30 43 42.1	18.77	49665	15	emiss
12 55 14.96	-29 21 42.9	18.24	16163	29	
12 55 15.01	-29 25 10.8	19.02	24705	36	
12 55 16.26	-29 33 12.8	19.19	24584	69	
12 55 17.00	-29 50 44.7	18.84	31938	57	
12 55 17.99	-29 24 22.8	18.74	41819	44	
12 55 18.45	-29 52 47.1	18.73	31229	34	
12 55 18.69	-29 26 28.1	16.98	24697	31	
12 55 19.23	-30 31 42.4	18.88	17052	51	
12 55 19.37	-29 20 51.0	19.21	24541	47	
12 55 19.37	-29 08 43.2	18.23	21359	90	emiss
12 55 19.47	-29 17 17.6	17.76	16623	33	
12 55 19.77	-29 35 50.6	19.15	17876	43	
12 55 20.23	-29 51 28.6	18.61	31156	36	
12 55 20.81	-30 13 53.1	17.78	15934	33	
12 55 20.95	-29 04 44.5	18.54	20813	41	
12 55 21.61	-29 52 30.8	18.42	25973	36	
12 55 21.62	-30 18 04.1	18.79	15000	44	
12 55 22.22	-29 23 52.8	18.05	28785	43	
12 55 22.82	-29 01 24.8	18.19	16319	81	
12 55 22.89	-29 45 34.0	18.54	38722	73	
12 55 22.90	-30 38 27.9	18.75	16459	69	
12 55 23.30	-30 26 52.2	19.22	23093	44	
12 55 23.88	-30 35 06.8	17.16	23076	80	
12 55 24.71	-30 13 49.3	19.14	31800	32	
12 55 24.71	-30 20 05.3	18.75	15440	55	
12 55 24.74	-30 24 14.4	19.15	16900	31	
12 55 25.02	-29 22 17.3	17.67	24441	34	
12 55 25.14	-29 24 01.0	18.22	28949	50	
12 55 25.23	-29 26 44.7	18.61	41776	43	
12 55 25.26	-29 23 15.6	19.03	28975	52	
12 55 25.35	-29 17 26.6	18.39	17819	39	
12 55 25.50	-30 25 33.7	17.53	18229	54	
12 55 26.18	-29 33 32.0	18.06	16159	41	
12 55 26.18	-29 03 23.7	17.37	21462	50	
12 55 26.31	-30 34 31.4	17.69	16118	35	
12 55 27.59	-29 27 18.5	19.04	15425	31	
12 55 30.04	-29 25 43.2	18.94	28756	84	
12 55 30.05	-30 27 24.9	19.02	17170	31	
12 55 30.47	-29 40 29.7	18.87	20398	76	emiss
12 55 30.54	-30 12 35.8	18.96	31886	80	
12 55 30.87	-31 00 16.2	18.96	16707	71	
12 55 30.99	-30 28 15.3	18.85	15933	75	emiss
12 55 31.01	-29 22 09.3	17.47	16786	35	
12 55 31.40	-30 19 07.3	16.87	13849	41	
12 55 31.72	-30 21 30.5	18.50	16308	33	
12 55 31.74	-30 25 37.6	18.50	15922	51	
12 55 32.99	-31 15 18.7	17.25	16834	15	emiss
12 55 33.11	-30 24 55.1	18.84	16996	15	emiss
12 55 33.60	-29 55 57.1	17.88	16341	30	
12 55 33.72	-29 00 32.1	17.62	20961	47	
12 55 33.98	-29 32 48.0	19.21	24486	16	emiss
12 55 35.13	-29 18 55.5	19.28	28877	15	emiss
12 55 35.58	-30 13 18.9	17.48	16667	45	

Table 2. cont.

α (2000)	δ (2000)	b_J	v (km/s)	err	notes
12 55 36.44	-30 32 03.0	18.01	16768	35	
12 55 37.90	-30 20 28.2	19.09	15649	60	
12 55 39.03	-30 26 30.9	18.88	18294	38	
12 55 39.28	-30 59 43.0	18.11	15156	79	
12 55 39.89	-29 03 32.7	18.84	30808	114	
12 55 40.03	-30 02 16.4	17.52	15568	38	
12 55 40.15	-28 49 43.0	17.45	22686	45	
12 55 42.10	-30 12 49.5	19.04	17134	36	
12 55 42.41	-30 27 58.2	17.93	17147	39	
12 55 42.43	-30 41 53.8	18.53	15997	33	
12 55 42.47	-29 33 17.2	17.17	7370	44	
12 55 42.72	-29 30 26.1	18.03	16375	29	
12 55 42.95	-30 43 06.9	16.16	15451	39	
12 55 43.47	-29 24 41.3	17.02	28927	73	
12 55 44.30	-30 24 19.0	17.84	16004	46	
12 55 44.64	-29 22 32.2	18.86	14855	90	emiss
12 55 44.72	-29 01 12.0	18.19	16611	57	
12 55 45.60	-30 24 52.9	18.32	16162	75	
12 55 45.62	-30 03 24.3	18.19	15623	60	
12 55 48.18	-30 23 23.6	18.78	16652	50	
12 55 48.90	-30 21 33.6	17.91	16536	32	
12 55 49.45	-30 33 58.8	18.87	15449	60	
12 55 49.59	-30 14 08.0	17.44	16398	52	
12 55 49.90	-30 26 44.3	18.30	15250	51	
12 55 50.03	-30 39 37.0	18.74	17097	40	
12 55 50.74	-28 45 15.8	18.02	16381	40	
12 55 51.71	-31 18 51.0	17.58	15839	32	
12 55 51.83	-30 00 28.4	18.17	16840	28	
12 55 51.96	-28 46 59.6	18.35	16178	15	emiss
12 55 52.53	-29 41 29.2	19.10	16132	41	
12 55 52.67	-30 25 32.6	18.21	16274	31	
12 55 53.25	-30 13 04.7	18.85	16808	56	
12 55 53.32	-31 07 31.5	18.60	16048	33	
12 55 53.48	-30 27 25.0	17.32	16174	29	
12 55 53.93	-30 17 28.4	19.04	16130	15	emiss
12 55 54.01	-31 18 12.3	18.48	16176	40	
12 55 54.04	-31 19 27.2	17.14	16128	34	
12 55 54.18	-30 21 42.0	18.52	17451	33	
12 55 54.50	-31 09 09.3	17.38	16609	34	
12 55 55.03	-30 23 47.0	18.79	15825	44	
12 55 55.06	-30 43 17.2	16.20	16753	30	
12 55 55.35	-30 15 54.4	18.03	16623	32	
12 55 56.07	-29 07 15.4	18.68	31080	66	emiss
12 55 56.82	-29 58 58.6	18.09	17073	35	
12 55 57.02	-29 55 40.0	18.41	16915	37	
12 55 57.17	-31 23 15.8	17.66	16790	44	
12 55 57.52	-29 17 58.4	17.15	16784	41	
12 55 58.55	-30 25 43.1	17.92	16418	29	
12 55 58.95	-29 44 48.2	17.87	16785	62	
12 55 59.37	-29 20 43.5	18.78	20440	75	
12 55 59.82	-29 39 39.0	19.23	16486	77	
12 55 59.92	-30 00 01.9	17.78	16044	15	emiss
12 56 00.28	-29 35 47.3	18.83	16099	40	
12 56 01.55	-30 58 42.3	18.72	16573	38	
12 56 02.14	-29 36 10.7	18.95	16107	81	
12 56 02.49	-30 50 04.6	18.34	16535	51	
12 56 03.76	-29 42 52.7	17.20	4882	66	emiss
12 56 04.36	-30 42 02.2	18.13	17022	37	
12 56 04.46	-30 26 27.8	18.30	15503	39	
12 56 04.69	-31 05 06.0	18.35	16640	39	
12 56 04.70	-31 25 57.8	18.49	16734	85	
12 56 05.40	-29 27 23.1	17.88	25628	33	
12 56 06.29	-30 20 19.9	18.61	17586	37	

Table 2. cont.

α (2000)	δ (2000)	b_J	v (km/s)	err	notes
12 56 07.07	-29 54 15.4	17.91	16442	28	
12 56 09.09	-31 19 34.7	17.57	17251	80	
12 56 10.39	-29 37 19.5	18.80	15303	43	
12 56 10.77	-30 39 08.0	18.55	15829	35	
12 56 11.19	-30 44 07.6	18.44	15482	66	emiss
12 56 12.12	-29 52 00.0	17.70	17081	31	
12 56 12.35	-29 02 57.4	18.33	16169	108	
12 56 12.37	-31 18 29.5	18.17	16905	37	
12 56 12.92	-30 08 58.5	16.94	15336	37	
12 56 13.54	-29 37 56.6	18.03	15261	62	
12 56 13.64	-30 36 01.7	18.54	17341	41	
12 56 13.79	-30 44 51.1	18.37	16728	30	
12 56 13.79	-31 06 52.3	16.97	16579	33	
12 56 13.97	-30 23 08.5	17.62	4684	15	emiss
12 56 15.16	-30 47 55.4	18.29	15504	54	
12 56 16.31	-30 41 53.5	18.03	4750	15	emiss
12 56 16.73	-29 59 04.1	18.62	25102	16	emiss
12 56 17.74	-29 09 07.8	18.31	16736	69	
12 56 17.94	-30 38 04.8	17.47	28270	34	
12 56 18.12	-30 03 48.3	18.94	17424	61	
12 56 19.14	-30 57 33.3	18.03	16670	25	
12 56 20.22	-30 40 16.4	17.42	15327	39	
12 56 20.64	-30 52 24.6	18.78	16973	38	
12 56 20.73	-31 11 49.1	17.85	17611	33	
12 56 20.78	-28 59 14.4	16.63	18041	89	
12 56 20.80	-31 14 46.6	18.12	18190	44	
12 56 21.28	-28 50 11.1	18.84	22115	15	emiss
12 56 21.92	-28 55 01.8	18.28	29616	73	
12 56 22.42	-31 17 19.9	17.88	16970	62	emiss
12 56 23.36	-29 33 46.8	18.90	15236	91	
12 56 23.71	-30 15 25.6	18.51	15212	83	emiss
12 56 24.15	-30 40 09.2	17.93	16904	41	
12 56 24.80	-31 25 58.7	18.36	15776	68	
12 56 24.86	-30 05 28.9	18.64	16948	32	
12 56 25.33	-30 13 21.6	17.95	31929	35	emiss
12 56 27.01	-29 27 27.1	18.98	17780	59	
12 56 27.11	-30 31 37.4	18.58	15950	31	
12 56 27.25	-29 01 34.5	18.25	18053	36	
12 56 27.39	-31 27 08.2	15.86	15671	30	
12 56 27.77	-29 06 26.6	18.67	20728	15	emiss
12 56 27.91	-31 17 08.6	16.97	17183	34	
12 56 28.02	-30 23 39.9	18.19	16016	37	
12 56 28.72	-31 23 26.0	18.58	17502	31	
12 56 29.14	-29 51 21.3	18.64	15302	91	emiss
12 56 29.94	-29 53 03.1	18.65	17189	59	
12 56 30.25	-31 17 45.0	18.44	16691	28	
12 56 31.73	-30 38 13.8	17.64	16980	34	
12 56 31.99	-30 17 42.2	18.65	16057	51	
12 56 32.25	-31 24 05.9	18.09	16383	36	
12 56 32.59	-28 57 12.8	18.51	17728	53	
12 56 33.39	-30 30 08.7	18.60	16390	34	
12 56 33.58	-31 03 50.4	17.77	17451	35	
12 56 34.15	-30 07 45.7	17.88	14889	37	
12 56 36.54	-29 55 15.3	18.89	52587	77	
12 56 37.99	-30 27 50.3	18.44	16536	30	
12 56 38.34	-30 47 58.6	18.81	15201	37	
12 56 38.78	-30 10 29.2	16.74	15965	28	
12 56 39.09	-30 51 41.6	17.43	15534	37	
12 56 39.29	-31 01 29.1	18.71	15382	77	
12 56 39.88	-30 07 20.4	18.88	24592	79	
12 56 40.76	-29 52 23.1	18.11	16643	63	
12 56 40.85	-31 03 19.6	17.46	17175	26	
12 56 40.93	-31 20 19.1	17.39	17200	30	

Table 2. cont.

α (2000)	δ (2000)	b_J	v (km/s)	err	notes
12 56 42.13	-29 45 26.4	18.59	16970	89	emiss
12 56 42.96	-30 01 12.7	17.75	16798	33	
12 56 43.23	-30 44 59.3	17.36	16198	32	
12 56 43.57	-30 14 32.4	18.07	16778	28	
12 56 44.81	-30 41 48.8	18.53	16062	41	
12 56 44.97	-31 01 29.8	18.18	24663	40	
12 56 46.40	-30 32 23.1	17.30	16332	39	
12 56 47.12	-29 42 17.7	18.12	16094	69	
12 56 48.43	-30 37 41.2	18.40	20709	35	
12 56 48.77	-28 48 54.2	18.79	20658	15	emiss
12 56 50.09	-31 14 05.2	18.44	18521	40	
12 56 50.28	-28 50 47.2	17.64	15406	40	
12 56 50.57	-30 14 25.8	17.90	17023	27	
12 56 51.10	-29 07 44.8	18.19	72708	43	
12 56 51.51	-30 48 54.4	18.78	16190	33	
12 56 51.63	-28 48 44.9	18.86	20249	47	
12 56 51.88	-30 47 40.7	17.56	16130	31	
12 56 52.57	-29 09 55.6	18.01	24567	63	
12 56 53.67	-31 31 43.3	17.40	15896	58	
12 56 54.82	-31 27 15.1	16.74	16033	35	
12 56 55.27	-29 11 03.6	18.52	16209	128	
12 56 56.60	-31 13 47.0	18.30	26402	69	emiss
12 56 57.39	-30 30 08.4	17.99	15145	31	
12 56 57.40	-28 56 22.4	17.79	16681	63	
12 56 57.41	-30 24 45.6	18.53	17235	37	
12 56 57.86	-28 59 07.6	18.00	15562	52	
12 56 58.09	-31 19 47.0	14.80	16881	42	
12 56 58.36	-30 06 04.6	18.57	17162	15	emiss
12 56 58.72	-31 22 08.8	18.19	17077	39	
12 57 00.77	-29 57 04.8	17.33	17469	41	
12 57 02.30	-30 19 26.3	18.37	18197	33	
12 57 02.78	-29 55 22.6	18.93	16875	15	emiss
12 57 03.08	-28 36 29.2	18.75	20087	91	
12 57 04.30	-28 54 24.4	18.10	17870	15	emiss
12 57 08.63	-30 01 36.2	18.09	16617	15	emiss
12 57 08.82	-31 18 58.4	16.97	15621	32	
12 57 09.52	-29 03 02.7	16.93	18320	55	
12 57 11.37	-31 15 59.4	17.55	16700	31	
12 57 11.44	-30 21 30.2	18.50	17158	45	
12 57 11.55	-28 26 03.5	18.68	20886	39	emiss
12 57 12.06	-28 56 45.7	17.66	15485	47	
12 57 12.25	-29 01 55.6	18.40	21137	55	
12 57 12.83	-31 11 12.5	18.57	15522	50	
12 57 13.23	-28 47 37.0	17.06	20159	37	
12 57 13.58	-28 53 49.3	18.26	24433	68	emiss
12 57 14.45	-30 20 26.2	17.66	14347	40	
12 57 15.22	-28 22 33.0	18.12	20750	59	
12 57 15.94	-28 45 17.1	18.38	24585	70	emiss
12 57 16.09	-29 56 23.4	17.42	17426	65	
12 57 16.69	-29 00 54.9	18.33	41439	79	
12 57 16.76	-31 16 10.3	18.04	16414	36	
12 57 17.39	-30 21 11.9	18.20	16990	24	
12 57 17.99	-30 48 07.9	18.80	22762	80	emiss
12 57 18.09	-28 44 17.0	16.60	20624	61	
12 57 18.14	-29 55 12.6	17.57	17200	83	emiss
12 57 20.22	-31 11 21.6	18.05	16575	31	
12 57 21.30	-28 30 21.2	17.23	20096	25	
12 57 21.84	-31 23 53.7	16.61	17815	61	
12 57 22.00	-29 53 14.4	17.40	3110	15	emiss
12 57 23.48	-30 27 19.2	18.54	16999	35	
12 57 23.82	-30 19 56.9	18.10	15602	33	
12 57 24.20	-28 42 14.8	18.28	19816	29	
12 57 24.41	-28 32 25.6	18.37	16960	28	

Table 2. cont.

α (2000)	δ (2000)	b_J	v (km/s)	err	notes
12 57 24.65	-29 03 44.0	17.24	18160	62	emiss
12 57 26.87	-30 21 28.8	18.41	16872	36	
12 57 27.40	-30 35 52.2	17.89	16721	29	
12 57 28.45	-29 00 20.5	16.82	18745	15	emiss
12 57 30.65	-28 38 08.9	18.65	20310	19	emiss
12 57 31.67	-31 21 01.5	14.84	7486	40	emiss
12 57 32.97	-29 02 30.2	18.25	22723	15	emiss
12 57 33.65	-31 21 35.5	18.10	16623	41	
12 57 34.88	-28 18 55.9	18.58	23010	46	emiss
12 57 34.92	-29 01 49.3	17.25	17709	70	
12 57 36.11	-28 38 33.4	18.60	19674	43	
12 57 39.21	-28 27 55.2	17.21	4998	95	emiss
12 57 39.29	-30 20 40.3	18.17	16197	49	
12 57 39.57	-28 31 21.3	18.53	20109	81	
12 57 39.98	-31 12 13.5	18.50	22935	57	emiss
12 57 41.08	-28 24 22.6	19.32	19749	105	emiss
12 57 43.25	-28 35 33.8	18.65	19602	32	
12 57 43.78	-28 25 02.7	19.27	20151	95	
12 57 44.56	-28 38 56.2	18.80	40905	76	
12 57 46.12	-31 17 36.5	18.45	16704	33	
12 57 46.52	-28 31 40.9	19.01	20105	96	
12 57 46.91	-28 32 28.1	17.61	20279	32	
12 57 47.24	-28 30 56.2	19.18	20626	89	
12 57 47.46	-28 31 20.1	18.58	20983	56	
12 57 48.40	-28 30 08.7	18.49	19960	43	
12 57 48.77	-28 18 56.3	18.78	19892	145	emiss
12 57 49.33	-28 31 20.6	16.84	20142	31	
12 57 49.57	-28 34 55.1	17.10	17123	57	emiss
12 57 50.05	-28 28 13.9	16.84	19970	51	
12 57 51.18	-28 40 59.2	19.11	16977	193	emiss
12 57 51.90	-28 28 59.2	19.35	19623	97	
12 57 52.97	-28 27 35.6	18.21	19547	53	
12 57 53.31	-28 19 37.8	18.39	20166	44	
12 57 53.33	-30 15 33.3	17.96	9496	90	
12 57 53.55	-28 25 22.6	17.19	20094	91	emiss
12 57 56.26	-28 30 21.5	18.76	14568	118	emiss
12 57 57.06	-28 19 44.7	19.17	20562	132	
12 57 57.20	-28 16 02.5	19.13	65710	113	
12 57 57.52	-28 20 03.6	18.11	20382	133	emiss
12 57 57.72	-30 19 33.1	18.49	16952	84	emiss
12 57 57.85	-28 25 23.6	17.55	17083	54	
12 57 57.95	-28 17 20.3	19.22	23843	87	
12 58 00.33	-28 28 15.2	18.63	17026	36	
12 58 01.03	-28 17 52.1	19.14	19919	17	emiss
12 58 02.10	-28 25 43.4	19.31	22527	109	emiss
12 58 03.60	-28 19 56.5	18.60	19909	51	
12 58 04.28	-28 32 54.2	19.35	20942	115	emiss
12 58 05.68	-28 17 03.8	17.93	19736	22	emiss
12 58 06.16	-28 17 50.4	18.48	19674	62	
12 58 07.12	-30 28 11.2	17.61	22754	12	emiss
12 58 09.40	-28 28 25.4	19.40	20370	83	
12 58 13.71	-28 29 21.9	19.22	20396	200	emiss
12 58 14.02	-28 38 09.7	19.08	40658	122	emiss
12 58 15.50	-28 16 20.4	17.84	23416	61	
12 58 19.32	-28 32 33.2	18.73	20094	104	emiss
12 58 20.66	-28 30 13.4	18.32	20731	43	
12 58 20.92	-28 36 15.1	19.22	20208	98	emiss
12 58 23.24	-28 14 50.4	18.90	22484	123	emiss
12 58 24.08	-28 29 29.5	17.72	20444	36	
12 58 24.89	-28 40 54.6	18.46	19183	86	emiss
12 58 26.56	-28 16 45.1	18.38	23148	68	
12 58 26.71	-28 29 43.8	17.05	20719	39	
12 58 29.00	-28 37 13.8	18.28	20379	48	

Table 2. cont.

α (2000)	δ (2000)	b_J	v (km/s)	err	notes
12 58 31.92	-28 32 53.8	18.61	40941	81	emiss
12 58 36.56	-28 29 42.5	19.09	32533	47	emiss
12 58 37.94	-28 41 33.7	18.40	19344	44	emiss
12 58 39.65	-28 37 27.7	17.05	21062	57	
12 58 39.91	-28 15 27.9	17.93	19528	116	
12 58 40.52	-28 28 45.8	17.58	20928	13	emiss
12 58 41.30	-28 41 18.8	19.04	31627	201	
12 58 42.49	-28 32 54.6	19.17	41215	165	emiss
12 58 43.41	-28 33 10.0	17.45	20823	71	
12 58 43.64	-28 24 06.3	19.06	20619	57	emiss
12 58 55.02	-28 38 15.4	18.59	20706	155	emiss
12 58 57.67	-28 23 54.5	19.30	60140	49	emiss
12 59 01.74	-28 33 15.9	19.25	15830	79	emiss
12 59 12.39	-28 23 58.5	19.15	60356	35	